Visualizing Natural Image Statistics

Hui Fang, Gary K. L. Tam, *Member, IEEE*, Rita Borgo, Andrew J. Aubrey, *Member, IEEE*, Philip W. Grant, *Member, IEEE*, Paul L. Rosin, Christian Wallraven, Douglas Cunningham, David Marshall, *Member, IEEE*, and Min Chen, *Member, IEEE*

Abstract—Natural image statistics is an important area of research in cognitive sciences and computer vision. Visualization of statistical results can help identify clusters and anomalies as well as analyze deviation, distribution and correlation. Furthermore, they can provide visual abstractions and symbolism for categorized data. In this paper, we begin our study of visualization of image statistics by considering visual representations of power spectra, which are commonly used to visualize different categories of images. We show that they convey a limited amount of statistical information about image categories and their support for analytical tasks is ineffective. We then introduce several new visual representations, which convey different or more information about image statistics. We apply ANOVA to the image statistics to help select statistically more meaningful measurements in our design process. A task-based user evaluation was carried out to compare the new visual representations with the conventional power spectra plots. Based on the results of the evaluation, we made further improvement of visualizations by introducing composite visual representations of image statistics.

Index Terms—Image statistics, image visualization, usability study, visual design.

1 INTRODUCTION

Natural image statistics are collections of statistical measurements that characterize, in some way, certain visual attributes of images captured from nature. It has been an area of interest in cognitive science and computer vision for over three decades (e.g., [7], [13], [23], [28], [32], [33]). Since humans have little difficulty in classifying scenes [33] and recognizing objects, Rosch *et al.* [28] hypothesized that there might be basic processes in the human vision system corresponding to gathering particular statistical measurements. The research of these statistical measurements has led to natural image statistics, which are found to have applications in many areas including content-based image retrieval [16], object detection [10], image compression [1], realism of computer synthesized imagery [26] and visualization of image databases.

Statistics can often benefit from effective visualization and in this paper we investigate the visualization of natural image statistics. Typical visualization techniques used to display image statistics, include bar charts, scatter plots, line plots, pixel-based visualization and 3D surfaces (Fig. 1). Such visual representations can support analytical tasks (e.g., cluster and anomaly identification; deviation, distribution and correlation analysis) and provide visual abstractions and symbolism. As an example, Fig. 2 shows ten line plots for different categories of images. Such plots are commonly referred to as *spectral signatures* [32] (for more on spectral signatures, see Section 2.1), one of the important statistical properties of images.

H. Fang, R. Borgo, P. W. Grant are with Swansea University, E-mail: {h.fang, r.borgo, p.w.grant}@swansea.ac.uk
G. K. L. Tam, A. J. Aubrey, P. L. Rosin and D. Marshall are with Cardiff University, E-mail: {kwok-leung.tam, a.j.aubrey, paul.posin, dave.marshall}@cs.cardiff.ac.uk
C. Wallraven is with Department of Brain and Cognitive Engineering, Korea University, E-mail: christian.wallraven@tuebingen.mpg.de
D. Cunningham is with Brandenburg Technical University, Germany. E-mail: douglas.cunningham@tu-cottbus.de
M. Chen is with University of Oxford, E-mail: min.chen@oerc.ox.ac.uk

In this work, we will address the following two questions.

(a) How well can such abstract visualizations support the above mentioned analytical tasks?
(b) Can we design more effective visual abstractions and symbolism for natural image statistics?

To answer (a), we use several conventional visualization techniques to study the correlation between the spectral signatures and the underlying classification of images. We show that spectral signatures encode very limited statistical measurements and cannot support identification of clusters and anomalies nor analysis of deviation, distribution and correlation (see Section 4). To answer (b), we first establish a set of criteria for designing the visual representations. We then employ the ANOVA statistical procedure, in conjunction with visualization, to identify informative statistical measurements (see Section 5). This enables us to select a subset of measurements to be encoded in the new visual representations. Our new visual representations exhibit compactness in visual display, facilitating visual abstraction and symbolism as well as richness in information content, providing more effective support for analytical tasks (see Section 6). A task-driven user study was carried out to evaluate the new representations, confirming the relative merits of these designs. In Section 7 we introduce a further collection of new composite designs based on the outcomes of the user study. A subsequent user study shows that these modified visualizations provide even better support for a variety of analytical tasks. We present our concluding remarks in Section 8.

2 RELATED WORK

In this section, we survey the related research and show how our work differs from existing approaches in the literature.

2.1 Natural Image Statistics

Natural image statistics uses methods and measurements to discover particularly interesting regularities and patterns in

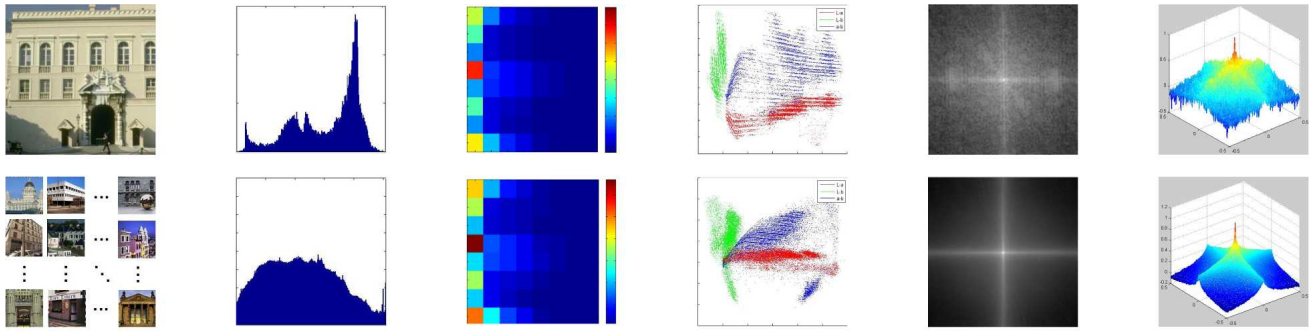

(a) Images (b) Histogram (c) Gradient hist (d) Lab space (e) FFT, 2D (f) FFT, 3D

Fig. 1: Typical visualizations of image statistics for a single image (top row) and a category of images (bottom row). For the images in (a), the techniques shown are: (b) area plots of intensity histograms, (c) pixel-based gradient histograms (with magnitude and orientation as axes), (d) scatter plots of color distribution in Lab space, (e) pixel-based visualization of Fourier power spectra, and (f) 3D surface representations of power spectra.

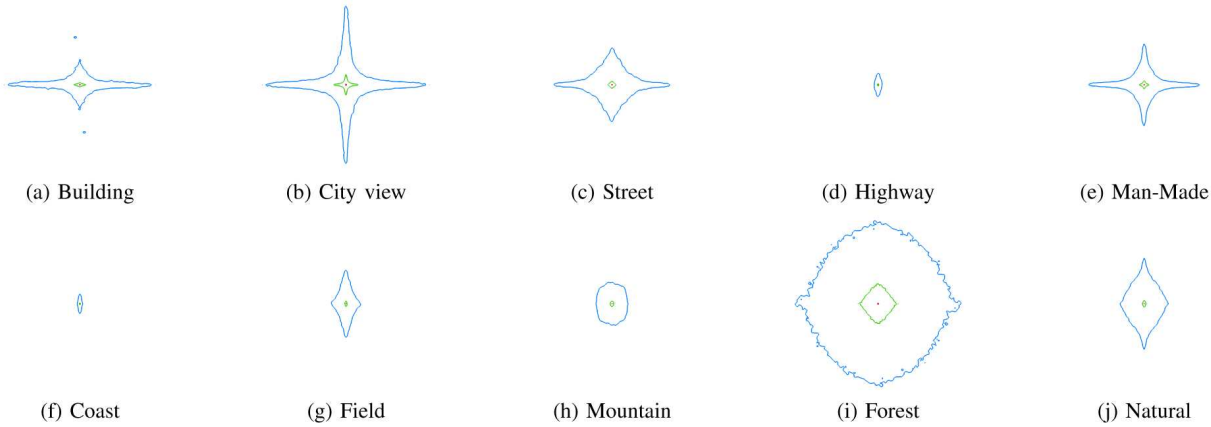

(a) Building (b) City view (c) Street (d) Highway (e) Man-Made

(f) Coast (g) Field (h) Mountain (i) Forest (j) Natural

Fig. 2: Contour representations of Fourier power spectral signatures.

sets of images. A recent survey [23] provides an up-to-date review of the state of the art. Image statistics can be obtained from many different sources, such as gray-level images, color images, range images or videos [8]. The simplest statistical descriptions are extracted from gray-level images. Although they include less information compared to that from color images, for many human or computer vision tasks (e.g., navigation, recognition) gray scale images contain most of the salient information. In many color-space transforms (e.g., Lab, YUV, YCbCr) greater emphasis is often made, via chroma subsampling, of the luminance (gray scale) component over the color components (e.g., in JPEG/MPEG compression).

The Fourier power spectrum is a popular transform space for statistical analysis. It has been shown that the spectral power, averaged over many images, varies as a power of the inverse frequency ($1/f^n$) [34]. In [11], the power spectra of Fourier spatial frequencies is visualized by using tree maps to show this pattern. In [32], Torralba *et al.* found that, for different classes of scenes, the contour plots of the energy of power spectra at a series of thresholds have different (and sometimes distinctive) shapes. These contours can be used as symbolic glyph representations to help with scene classification [32]. In [31], Principal Component Analysis (PCA) coefficients, based on Fourier power spectra, are employed as features for scene depth estimation. Although the usefulness of these findings has been demonstrated, spectra of *individual* images are much more irregular as is mentioned in [32], but there has been little work on analyzing these variations.

Several analytical methods have been adopted to obtain statistical properties of images usually based on different assumptions. PCA assumes the data obeys a Gaussian distribution. Kernel Principal Component Analysis (KPCA) assumes a Gaussian distribution in a higher dimensional feature space where a kernel is applied to the data. Independent Component Analysis (ICA) assumes a non-orthogonal 2nd order statistics distribution of the underlying data (super-Gaussian). The choice of kernel can be critical. Where the data characteristics are not well known, this can be problematic. Different analytical methods can reveal different statistical characteristics inherent in the data. It is therefore desirable to depict multiple characteristics in appropriate visual representations.

2.2 Applications and Challenges

The most extensive use of image statistics is to help computer vision scientists discover the statistical descriptors for a specific category of objects or scenes (e.g., [28], [32], [33]). Image statistics have proved invaluable in gaining insight in computer graphics and image analysis. By computing and analyzing the statistics of different image ensembles, researchers have not only made discoveries about the correlation between a specific

set of statistical indicators and the desired perceptual quality of an image, but also have used these discoveries to develop advanced image manipulation techniques. For example, an improved understanding of the first order statistics of image ensembles enabled the transfer of statistical moments between images using histogram matching or color transfer (e.g., the color "atmosphere" of one image can be transferred to another) [25]. Understanding of the relationship between second order statistics and plant images led to improvement of graphical synthesis of plants [4]. The same is true for the synthesis of landscapes [27]. Analysis of image statistics helped discover the statistics that specify the reflectance of an object [5], while statistics about image blur and image noise were used in image de-blurring and denoising [6], [22].

In many situations, gaining insight from statistics is a non-trivial task. In image inpainting, for example, knowing what important statistics the missing texture should have is critical [18]. In transferring image characteristics, better understanding of image statistics and the correlation would help design better algorithms to capture and transfer those aesthetic properties [24]. Despite cultural prominence as canonical "stimuli", scientists only recently began to conduct more rigorous investigations into the statistics of imagery properties of artworks [9]. An important need is to allow quantification of artistic styles, which can lead to new tools for identifying forgeries or determining the source of a work of art [12].

Visualization has played a role in the analysis of image statistics. However, similar to earlier visualization in statistics, most researchers concentrated on primitive visual representations such as line plots and bar charts, and most are used to convey a specific form of simple statistics such as means, which provides limited support for the analysis of complex relationships between image ensembles and image statistics. Through our literature studies and our research experience on image statistics, we believe that the identification of complex statistical patterns of image ensembles in many applications can only become possible, or will at least be more effectual, by using novel visualization tools.

2.3 Visual Abstraction

Visualization has been used in image statistics. Fig. 1 shows a number of commonly-used visual representations. The first row shows five different visual representations of statistical properties of the image in (a). The histogram in column (b) shows the distribution of pixel intensities in the image. The pixel-based visualization in (c) is a 2D gradient histogram with magnitude and orientation as its two axes. In (d), the pixels in the source image are randomly sampled and the three Lab color space components of these pixels are paired up and plotted as red, green or blue. In (e) and (f), magnitudes of Fourier power spectra are visualized using a 2D pixel representation and a 3D surface respectively. The second row of Fig. 1 shows the average features, over all images in a class, computed from different transformed spaces corresponding to individual columns.

The most commonly-used visualization (e.g., [32]) for depicting a class of images is contour-based abstraction as shown in Fig. 2, where contours represent different power spectra energies. They are considered as spectral signatures serving as a form of symbolism. In [29], a radar graph approach is used to illustrate the image patterns in both low-frequency and high-frequency Gabor responses. If we draw an analogy between a radar graph and a bar chart (one of the most basic form of statistics visualization), each plot in Fig. 2 would be similar to a bar chart showing three statistical attributes of the sample population. When two populations are shown to have three similar (or different) scalar attributes, it may not be sufficient for one to say that the two populations are similar (or different). This leads to the need for an understanding about the effectiveness of such visualization in providing visual abstraction image categories and in supporting visual analysis of images and image classes.

As mentioned in [35], statistical inference can be achieved visually through visual representations containing statistical stimuli, such as tag clouds, tree maps, histograms and scatter plots, etc. In their work, two protocols, Rorschach and Line-up, are introduced to find the correct statistical inference with proper calibration and constraints. In our work, more attention is paid to how better visual designs can provide more information for comprehending image statistics.

3 Image Statistics

Let $A = \{a_1, a_2, \ldots, a_n\}$ be a very large collection of uncategorized images. We will use $X \subseteq A$, to denote any specific category of images that share a common set of attributes. For example, X may be a class of images that are predominated by a human face, or may be a class of forest scenes, etc.

Viewing the elements a_i in A as sets of *numbers*, many statistical functions could be applied to them, from simple summary statistics, such as mean, range and standard deviation, to more complex analytical operations (e.g., regression and correlation, etc.). Since each image, a_i, may be composed of thousands or millions of numbers, it is advantageous to map each image to a *few* representative quantities, where these mappings are usually statistical. Hence the term *image statistics* is used in two different contexts, that is, *class-level statistics* for examining the relationships between individual images and image classes, and *image-level statistics* for mapping an image to several quantities. In some cases, such as PCA, the statistics in these two levels are related to each other. We use $\mathscr{M}$, with one or two arguments, to denote a function that maps an image or a class of images to a statistical measurement, which will be used later for producing visual representations. When $\mathscr{M}$ is applied to an image $x \in X$ independently of other images, we denote this mapping as $\mathscr{M}(x)$. When $\mathscr{M}$ is applied to an image $x \in X$ in relation to all other images in the class, we denote such a mapping as $\mathscr{M}(x, X)$. In addition, we use function $T(x)$ to denote an image transform that is not considered as a statistical measurement.

3.1 Intensity, Color and Gradient Histograms

Histograms are simple image statistic measurements showing the distribution of values in an image. The function $\mathscr{M}_h$ transforms an image x to a small set of statistical quantities,

$[b_1, b_2, \ldots, b_m]$, which are the numbers of the values in each of the m bins. *Intensity histograms* focus on the luminance of pixels and count the number of pixels in each bin representing a luminance range. *Color histograms* extend the intensity histogram by encoding more distinctive information in three color channels. To compute a *gradient histogram* [2], first transform an image x into a gradient image $T_g(x)$, typically by computing central differences at each pixel position. The resultant gradient image $T_g(x)$ can then be mapped to a 1D histogram of gradient magnitudes in the image, a 1D histogram of gradient orientation, or a 2D histogram where bins are sorted by both magnitude and orientation. Hence, $[b_1, b_2, \ldots, b_m] = \mathscr{M}_h(T_g(x))$.

3.2 Fourier Power Spectral Signatures (FPSS)

Fourier power spectral signatures [32] are used in image statistics research. Given an image x, a 2D Fourier transformation is first applied to the image, resulting in a frequency domain representation $T_f(x)$. In the Fourier domain, the magnitudes of Fourier coefficients are calculated as a power spectral signature of the image x. The power spectrum, $\mathscr{M}_{fpss}(T_f(x))$, is a statistical measure of the power of the signal (energy per unit space) falling in different frequency bins. We will examine Fourier power spectral signatures in details in Section 4. It is assumed that FPSS in different resolutions may contain different useful information. We subdivide each image in a hierarchical manner and obtain FPSS contours for each subdivided image. This is referred to as a *scale space Fourier transform*.

3.3 Statistical Descriptors of Textures

Texture descriptors are a family of methods that capture statistics from textural patterns in images. Typically, an image x is subdivided into a collection of n pixel blocks, $[t_1, t_2, \ldots, t_n]$. A measurement of some visual features (e.g., homogeneity, orientation) is made on each block $t_k (k = 1, 2, \ldots, n)$, resulting in a quantity q_k that characterizes the block. The collection of these quantities, $[q_1, q_2, \ldots, q_n]$, yields a statistical descriptor of the image.

A commonly-used texture descriptors is based on Gabor filters [3]. An image x is subdivided into n texture blocks, denoted by the transformation $T_{div}(x)$. Each block t_k is convolved with a set of Gabor filters, $g_{i,j}, i = 1, \ldots, r, j = 1, \ldots, s$, covering r different orientations and s different scales. For each i, j, k the values in $g_{i,j}(t_k)$ are summed to produce a real value and these values yield a final image statistic $[\gamma_1, \gamma_2, \ldots, \gamma_{rsn}] = \mathscr{M}_\gamma(x)$. In our work, we used 4×4 image blocks, and a set of Gabor filters covering 8 orientations and 4 scales yielding, as a statistic, a vector of $4 \times 4 \times 8 \times 4 = 512$ real values.

3.4 Principal Component Analysis (PCA)

PCA [15] is typically applied to a collection of data, for example, a class of images $X = \{x_1, x_2, \ldots, \}$. It linearly transforms X to a new coordinate system so that the greatest variance of the data is encoded by the variance on the first few axes. The transformation requires the computation of a mean image $\overline{X}$, which can be considered a class-level statistics. The difference between each image x_i and $\overline{X}$, is then encoded by coefficients $[\rho_1, \rho_2, \ldots, \rho_c] = \mathscr{M}_{PCA}(x, X)$ corresponding to different eigenvectors.

Eigenvectors are typically sorted in descending order according to the corresponding eigenvalues. Thus, the first few eigenvectors of PCA are expected to capture the significant variance of the processed data and non-significant signals (possibly noise) lie on those eigenvectors with smaller eigenvalues. As a result, PCA is able to remove the noise from the data, while making use of fewer quantities (e.g., using only ρ_1 and ρ_2), to describe the images.

3.5 Kernel Principal Component Analysis (KPCA)

KPCA is an extension of PCA [17] obtained by introducing different kernels, such as linear kernels, radial basis function (RBF) kernels or polynomial kernels. The use of kernels allows one to solve only the eigenvectors and eigenvalues of a kernel, instead of a very high-dimensional feature space where other projection methods are used to map the data. In our work, a linear kernel is adopted as it is the only kernel that does not require any parameters to be tuned, so is a fully unsupervised statistical method.

3.6 Independent Component Analysis (ICA)

ICA [21] transforms a multivariate signal into a set of additive subcomponents which exhibit mutual statistical independence of non-Gaussian source signals. This is a form of *blind source separation* of a set of mixed signals into a set of statistically independent signals. A class of images, $X = \{x_1, x_2, \ldots, \}$ is a typical set of mixed signals. The goal of ICA is to obtain a mapping $\mathscr{M}_{ICA}$ so that a signal $x \in X$ can be transformed to a set of quantities $[\eta_1, \eta_2, \ldots, \eta_c] = \mathscr{M}_{ICA}(x, X)$. Typically one estimates $\mathscr{M}_{ICA}$ by minimizing mutual information, maximizing non-Gaussianity, or a combination of both [14].

4 Limitations of Spectral Signatures

Fourier power spectral signatures (FPSS) are widely used in semantic clustering tasks. High-frequency components of FPSS indicate sharp changes and texture details in images, while low-frequency components represent the main image structure, so FPSS can reflect different types of image patterns.

When original images are decomposed into Fourier space, geometrical structures are obtained by keeping certain amounts of energy in the frequency domain. Let p_i represent a point in the Fourier domain, and $f(p_i)$ the frequency response at this position. The total energy of an image is thus $E = \sum_{i=1}^{n} f(p_i)$. If τ is the percentage of energy to be retained, we can find a subset of points, $\{p'_1, p'_2, \ldots, p'_m\} (m \leq n)$ in the Fourier domain, such that $\tau E = \sum_{k=1}^{m} f(p'_k)$. To determine the subset, one typically sorts $p_i (i = 1, 2, \ldots, n)$ in the descending order of the values of $f(p_i)$, resulting in a sorted list $\{p'_1, p'_2, \ldots, p'_n\}$. One then adds each $f(p'_i)$ in the sorted list into a sum until the total sum equals or exceeds τE. The last value $f(p_m)$ added becomes a cut-off value c for τ. The plots in Fig. 2 show three contour lines representing cut-off points, c_1, c_2, c_3,

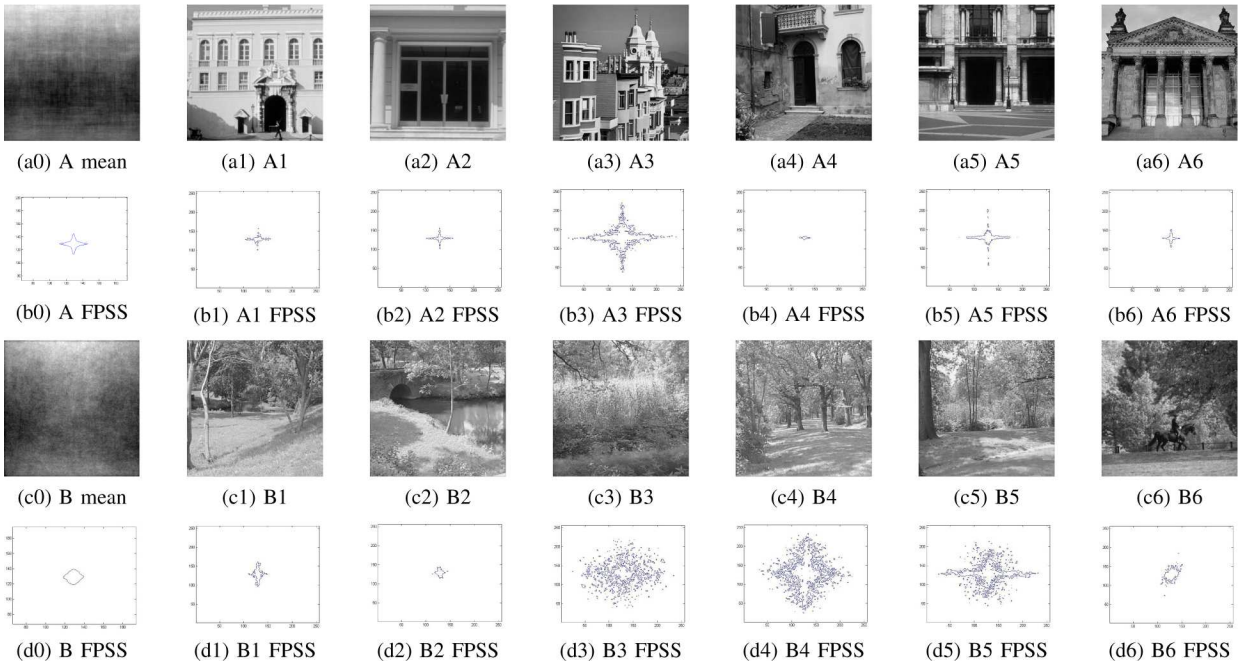

Fig. 3: Images from two different classes are not easily distinguishable using their Fourier power spectral signatures.

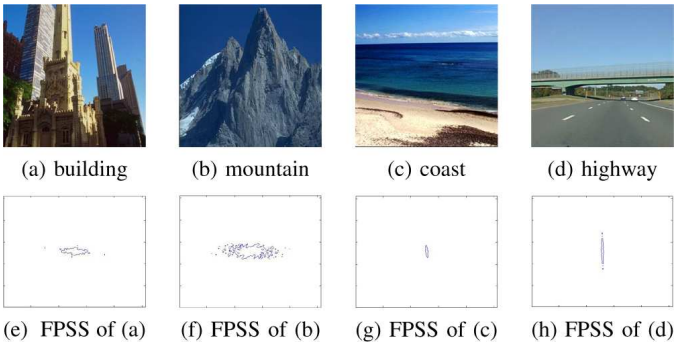

Fig. 4: Similar Fourier power spectral signatures.

corresponding to $\tau = 0.7, 0.8, 0.9$ respectively. The red line, c_1, consists of all points with their frequency responses $f(p_i) = c_1$, and the energy of all points on and inside the contour totals up to $70\%E$. Similarly, the green line corresponds to c_2 and $80\%E$, and the blue line corresponds to c_3 and $90\%E$.

Contours of an individual image are obtained when the image is transformed into frequency space, while contours of a class of images are calculated using the average frequency response over all images in the class.

In previous work, [20], [31], [32], such contours have been used to represent different classes of images (Fig. 2). However, contours of an image class are not representative for individual images in the class. We can see this from the wide variation of the contours in Fig. 3. Here images are randomly selected from two distinct classes [32]. Set A, (a1-a6), in are from the class *City View* and set B, (c1-c6), in are from the class *Forests*. The corresponding FPSS plots (b1-b6) and (d1-d6) are for 90% energy contours for individual images. (b0) is an FPSS plot for the average Fourier power spectra of the images in (a1-a6), while (d0) is that for (c1-c6). Note that (a0) and (c0), averages in the spatial domain, are not used in computing (b0) and (d0). Based on the plots in Fig. 3, it would be difficult to say, for example, A1 is in the *City View* class and B4 is in the *Forest*. On the other hand, two images from different classes may have similar contours if the main structures of the images bear a similarity with each other as shown in Fig. 4.

Distinctive FPSS contours for different classes (Fig. 2) could give a misleading impression that images in these classes would have rather different FPSS contours. It is difficult to define statistical criteria for classifying images in large image collections. For example, the class of *Building* has very distinctive FPSS contours in comparison with those of the class of *Forest*. However, the FPSS contours for individual images in the two classes are much less distinguishable. Using parallel coordinates with axial scatter plots (Fig. 5), we can visualize various statistical attributes of these two classes, including the first five PCA coefficients for several image statistics, including histogram, texture descriptor, gradient histogram and scale space Fourier transform. From the scatter plots, we see that the values of most attributes of the two classes have large overlaps, suggesting that to separate the two classes would require using statistical information based on *several* attributes.

Fig. 5 suggests that FPSS contours may mislead users into over-estimating how each image class is clustered and how it is separated from other classes. This is similar to plotting the means of different data sequences in a bar chart, without associating each bar with any information about data range, deviation, or distribution. Taking an FPSS contour plot for a single image, it is often difficult to correctly assign the image to its class. So, such visualizations offer limited support in data analysis, especially in supporting identification of clusters and anomalies, and analysis of deviation, distribution and correlation. This led us to design more informative visualizations, based on combining several statistical measures, to overcome some of the shortcomings of FPSS contours.

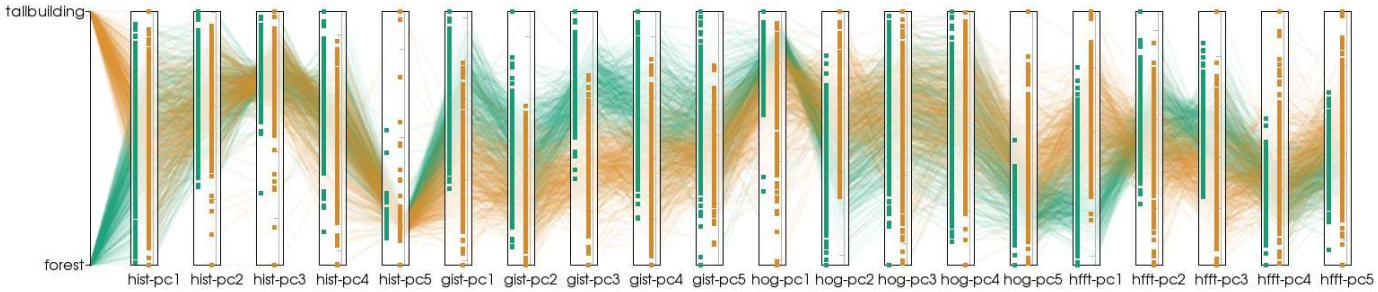

Fig. 5: Parallel coordinates with axial distribution plots show that it is difficult to separate images in the *Building* class from those in the *Forest* class, even though the FPSS contours for the two classes are distinctive as shown in Fig. 2.

5 Visual Design Process

The dataset used in our visual designs contains 2,688 images accessable from [30]. It has been widely employed as a benchmark dataset for scene categorization in the literature. Images are categorized into 8 scene classes: *Building*, *City View*, *Street*, *Highway*, *Coast*, *Field*, *Mountain* and *Forest*. Each of these classes has 356, 308, 292, 260, 360, 410, 374 and 328 pictures, respectively. The first four classes collectively form a superset *Man-Made* with 1216 images, and the other four form a superset *Natural* with 1472 images.

The visual design process in our work consisted of several stages: (i) the problem mentioned in Section 4 was identified and solution spaces discussed in a number of brainstorming sessions; (ii) visual designs were suggested starting with a study of the literature, followed by a large collection of design options; (iii) in several cases, analysis of variance (ANOVA) was used to optimize our designs (see Section 5.4); (iv) a user study was conducted to evaluate these options; and (v) refinement and enhancement with additional composite designs were proposed and evaluated (see Section 6).

As the criteria for guiding the design process and filtering design options, good visual representations should ideally:

(a) be a visual abstraction or glyph helping users identify and memorize common characteristics in each class;
(b) be capable of showing variations, deviation and distribution within each class;
(c) indicate relationships between classes, e.g., subset relationship, similarity and correlation;
(d) provide information to guide users to find the best classification based on properties, such as shape or size;
(e) make efficient use of space and different visual channels to convey more information;
(f) be aesthetically pleasing.

With these criteria in mind, over ten design options were proposed initially and finally narrowed down to three designs, which are detailed in the following subsections.

5.1 New Designs for FPSS

FPSS contours in [32] provide reasonable visual symbolism for representing different categories and they demonstrate some variability as required by criterion (b). However, they fail to satisfy criterion (c), and the variability of contours can be misleading. Several design options were thus proposed for visually fusing contours of all images in the class in a *distribution map*. A distribution map is a form of visualization, where a number of geometrical shapes that represent different data entities are spatially mapped to a shared domain. When there are a large number of such shapes, the shapes are usually displayed as translucent objects (e.g., in parallel coordinates visualization). The placement and density of these shapes hence indicate the distribution of the data entities.

Fig. 7 shows the distribution maps of the same 10 classes as in Fig. 2. For each class of images, instead of showing a representative contour in Fourier space, we display the contours of all images in the class using translucent black lines. In addition, we plot a representative contour in blue for the class at the 90% energy level.

Due to the symmetric characteristics of FPSS, signatures in the 1st quadrant are the same as those in the 3rd quadrant, and the 2nd quadrant is the same as the 4th. In addition, signatures in the 1st quadrant are usually quite similar to those in the 2nd. In some of our initial designs, such spatial redundancy was removed. For our main designs based on FPSS contours we choose the design with all 4 quadrants as it provides a balanced amount of information compared to other designs and is more aesthetically pleasing. In a later section, we also show the use of a design option without the redundant information.

5.2 New Designs for PCA, KPCA and ICA

PCA, KPCA and ICA are statistical methods which can be used for reducing dimensionality. Such methods result in statistical measurements in a parameter space. We experimented with several design options. The first option is a scatter plot, where each image is represented by a 2D point whose coordinates are two parameters of the chosen method. With different colors and different levels of transparency, the image points of a class (i.e., focus) are plotted against all other image points in the database (i.e., context).

This was evolved into the second option that uses a filled circle to enclose the whole data space (i.e., all images in the database), and further to the third option where the image points of the focus class was replaced with an ellipse. In addition, we introduced a circular grid as a spatial representation to support more effective comparison with other classes. As shown in Fig. 6(a), the circular data space is defined by its center ① (the average of all points), and 110% of the maximum radius ②. The ellipse is defined by the principal eigenvectors (spread) of a class, with its length equal to twice

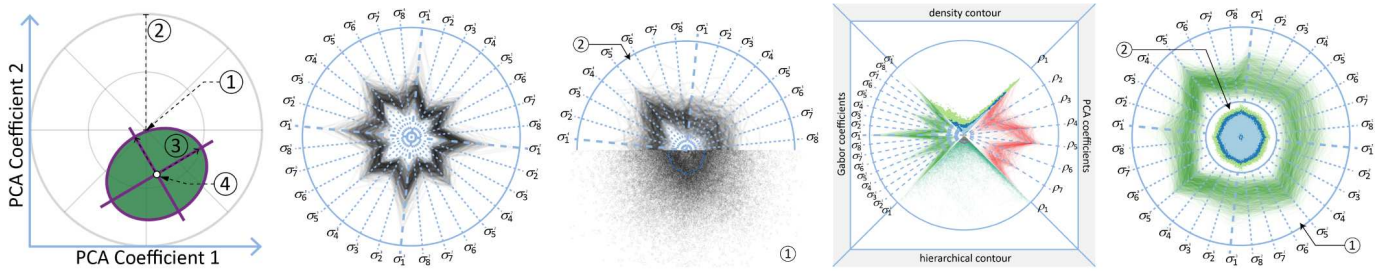

(a) PCA (b) Gabor (c) FPSS & partial Gabor (d) Gabor, PCA & FPSS (e) Gabor & quantized FPSS

Fig. 6: (a)-(b) PCA- and Gabor-based designs; (c)-(e) Three new combined visual designs proposed after the first user study.

the standard deviation ③. The class center ④ is the average of all points in a specific class. The three design options represent a transformation from a scatter plot to an an elliptic bubble plot. The visualization of 10 different classes using the third option is shown in Fig. 8.

5.3 New Design for Texture Descriptors

Ross *et al.* [29], use radii length representations to visualize Gabor-based texture descriptors. When an image is filtered by a set of Gabor filters, the mean response values are plotted in a radar graph. [29] claims that each image category has a distinctive pattern compared to each other. Similar to FPSS contours, it does not depict variations and distribution in a class, and the mean response values can be misleading.

Similar to the new design for FPSS, we display the texture descriptors of all images as a distribution map for an image class. As illustrated in Fig. 6(b), each of the 8×4 Gabor descriptors are plotted along the 32 radial axes. The descriptors of each image are connected circularly using translucent lines in a manner that is similar to parallel coordinates.

The full set of visual representations for the 10 classes is given in Fig. 9, where the characteristics of each class are more distinctive and noticeable in most cases. From the visualization, for instance, we can observe that the *Coast* and *Highway* classes have similar statistical properties. This confirms the existence of dominant horizontal structures in both types of images as exemplified by Figs. 4(c,d).

5.4 Steering Visual Designs using ANOVA

There are many methods for computing image statistics (see Section 3) and normally consist of two stages: an image feature space transform, e.g., histogram, FPSS and Gabor filters, followed by dimension reduction, such as PCA, etc. In our work, several sets of combinations are investigated. For example, $\mathscr{M}_{PCA}(\mathscr{M}_\gamma(x), \mathscr{M}_\gamma(X))$ is used for representations based on PCA applied to Gabor texture descriptors and $\mathscr{M}_{PCA}(\mathscr{M}_h(x), \mathscr{M}_h(X))$ for representations based on PCA parameters extracted from histogram vectors. However, PCA-based visual designs (in Section 5.2) are only suitable for depicting *two* parameters and there is a desire to avoid 3D visual designs for the design criterion (a) on abstraction and symbolism. It is therefore desirable to choose the most representative statistical attributes to create our visual representations. We thus turn to using Analysis of Variance (ANOVA) [19], which is capable of measuring the distinctive power and correlations between data sets or parameter sets. For our design process, we use ANOVA to help select two most representative statistical attributes from a large pool of measurements.

Fig. 10 shows a heatmap, depicting the ANOVA F-values of different statistical measurements. We considered applying ICA, PCA and KPCA to the vector results of the different methods (columns) mentioned in Section 3, taking the first twenty parameters in all cases. We found that when the Gabor descriptors are combined with PCA or KPCA, we can obtain parameters with high discriminative power. For PCA applied to Gabor descriptors, we see from Fig. 10 that p_1 and p_3 are the preferred choice and for KPCA the choice is p_2 and p_4. The design option shown in Fig. 8 depicts the values of p_1 and p_3 as the results of applying PCA to Gabor descriptors. Because the ordering of ICA, PCA or KPCA components depends on the variance between images, it does not correlate exactly with the order given by the ANOVA F-values that depend on the variance between different image classes.

6 Evaluation

After filtering various initial design options for visualizing image statistics based on the criteria discussed in Section 5, we arrived at three designs as shown in Figs. 7, 8 and 9.

We conducted a user study to see if any can be more informative and effective in supporting users' analytical tasks. In particular, we wanted to compare the three new designs with the original design based on FPSS contours as shown in Fig. 2.

Our pre-experiment hypotheses are:

- All three new designs (Figs. 7, 8 and 9) will be more helpful in determining *set memberships* of images than FPSS contours in Fig. 2.
- The PCA-based design (shown in Fig. 8) will be most effective in supporting the analysis of set relationship (e.g., *subset* and *distance*), while the other two new designs may marginally improve upon FPSS contours.

6.1 Participants

Twelve participants (5 female, 7 male) took part in this experiment in return for a £5 book voucher. All participants were recruited from the Swansea University community, 8 were students or post-doctoral researchers in Computer Science and 4 from the Business School. Their ages ranged from 19 to 41 (Mean=25.6, SD=5.83), and all had normal or corrected to normal vision. As the tasks of the user study involved

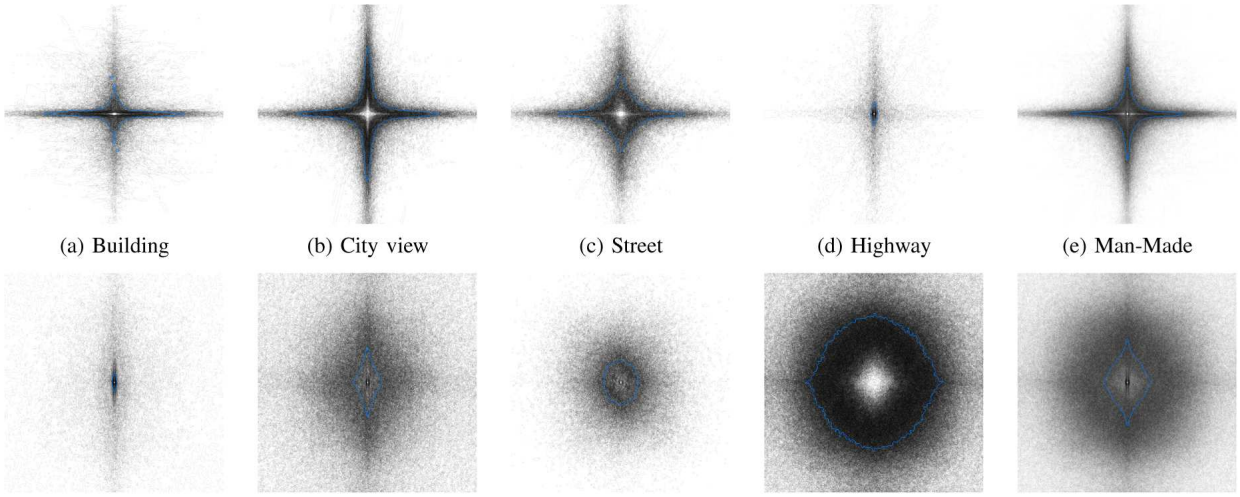

(a) Building (b) City view (c) Street (d) Highway (e) Man-Made

(f) Coast (g) Field (h) Mountain (i) Forest (j) Natural

Fig. 7: New visual representation of Fourier power spectral signatures.

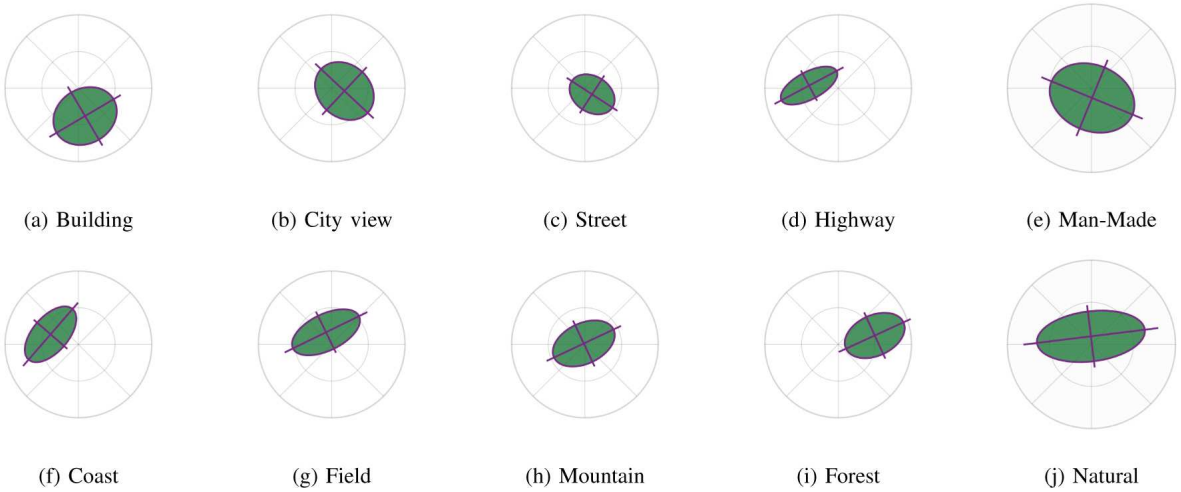

(a) Building (b) City view (c) Street (d) Highway (e) Man-Made

(f) Coast (g) Field (h) Mountain (i) Forest (j) Natural

Fig. 8: New visual representation of PCA measurements with highest ANOVA values.

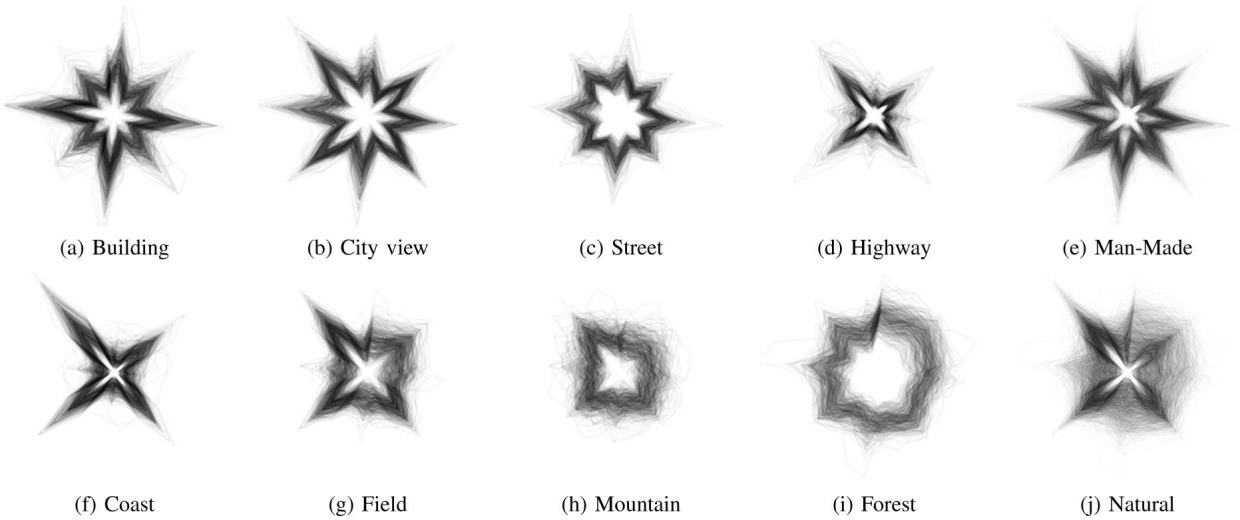

(a) Building (b) City view (c) Street (d) Highway (e) Man-Made

(f) Coast (g) Field (h) Mountain (i) Forest (j) Natural

Fig. 9: New visual representation of texture descriptors.

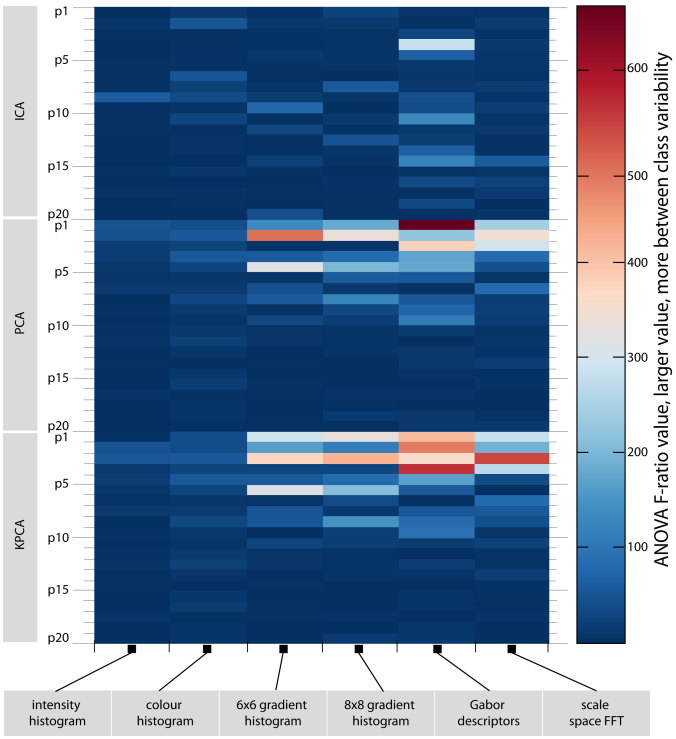

Fig. 10: Visualization of the discriminative power of a pool of statistical measurements.

FPSS Contour vs	Task 1	Task 2	Task 3	Task 4
FPSS Distribution Map	**.004**	.109	**.001**	.85
PCA-based Design	**.001**	**.002**	**.043**	.256
Gabor-based Design	**.002**	**.021**	**.032**	**<.001**
Combined Design 1	**<.001**	**.004**	**<.001**	**.005**
Combined Design 2	**<.001**	**.005**	**.005**	**<.001**
Combined Design 3	**<.001**	**.001**	**<.001**	**<.001**

TABLE 1: Pair-wise p-values of the old design vs. each of the new designs (values < 0.05 are in bold).

some understanding of the purpose of image statistics (but not algorithmic details), it was justifiable to have basic technical knowledge, such as understanding the meaning of 'subset' and 'parameter'. This was also a reasonable representation of the potential user groups of image statistics. All participants were informed about the purpose of the study at the beginning of the session, but not about any of our hypotheses. In particular, they were not made aware of whether any visual design is from the literature or newly created in this work.

6.2 Tasks and Variables

Participants were required to answer 112 questions (trials). The 112 questions were divided into four *task groups*, each with 28 questions. The four groups represented four different tasks. The 28 questions in each task group were further divided in 4 *design groups*, i.e. 7 questions for each of the four designs as shown in Figs. 2, 7, 8 and 9.

For Task 1, participants were given a set of stimuli consisting of visual representations of two image classes, A and B and one image X. Each participant was asked to determine if image X belongs to class A or B. All 28 questions in this task group were standardized as '*Which Image Class does Image X most likely belong to?*' The answers were either '*(a) Class A*' or '*(b) Class B*'.

For Task 2, participants were given a set of stimuli consisting of visual representations of one image class, A, and two images X and Y. All 28 questions in this task group were standardized as '*There is only one image, either X or Y, belongs to Class A. Which one?*' The answers were either '*(a) Image X*' or '*(b) Image Y*'.

For Task 3, participants were given a set of stimuli consisting of visual representations of two image classes, A and B. All 28 questions in this task group were standardized as '*Is Image Class B a subset of Image Class A?*' The answers were either '*(a) B *IS* a subset of A*' or '*(b) B *IS NOT* a subset of A*'.

For Task 4, participants were given a set of stimuli consisting of visual representations of three image classes, A, B and C. All 28 questions in this task group were standardized as '*Are images in Class C more similar to Images in Class A or B?*' The answers were either '*(a) A and C are more similar*' or '*(b) B and C are more similar*'. This is a difficult task, as the similarity between image classes is not well-defined. We included this task as a wild-card related to our second hypothesis. One common claim in the literature is that image statistics can separate the superset of *Man-Made* scenes from that of *Natural* scenes (e.g., [32]). The two reference classes (A and B) are chosen from two different supersets, one each. C is an image class from either superset.

All tasks represent typical use of natural image statistics. Tasks 1 and 2 are set membership determination, Task 3 is concerned with subset relationship, and Task 4 with set-based distance between different classes. Ground truth values of all tasks were based on the annotated classification in the database [30]. The independent variables are thus the four different visual designs as illustrated in Figs. 2, 7, 8 and 9, and the four different tasks mentioned above. The dependent variable is the correctness of the answers given by the participants.

6.3 Stimuli, Apparatus and Procedure

There were a total of 112 sets of stimuli, and each set consisted of 2 or 3 visualization images depending on individual tasks. The visual stimuli (i.e., visualization images) were created using software written in C++ and VTK. In addition to those shown in Figs. 2, 7, 8 and 9, a collection of visual representations were created for individual images to be used in Tasks 1 and 2. For Task 3, additional visual representations of two extra super-classes were created; *Land* (*Field* $\cup$ *Mountain* $\cup$ *Forest*), and *City* (*Building* $\cup$ *City View* $\cup$ *Street*).

Stimuli were saved as static images and presented to participants via custom software written in C++, with Qt as graphics library. We shuffled the 112 sets of questions to remove the natural grouping by either task or design. Because of the large number of questions of a similar nature, the order of the questions appears to be random. The placement of the correct answer also appears to be random in the trials.

Participants took part in the user study in groups of 2-4 people per session. Each experiment began with a brief overview read by the experimenter using a predefined script.

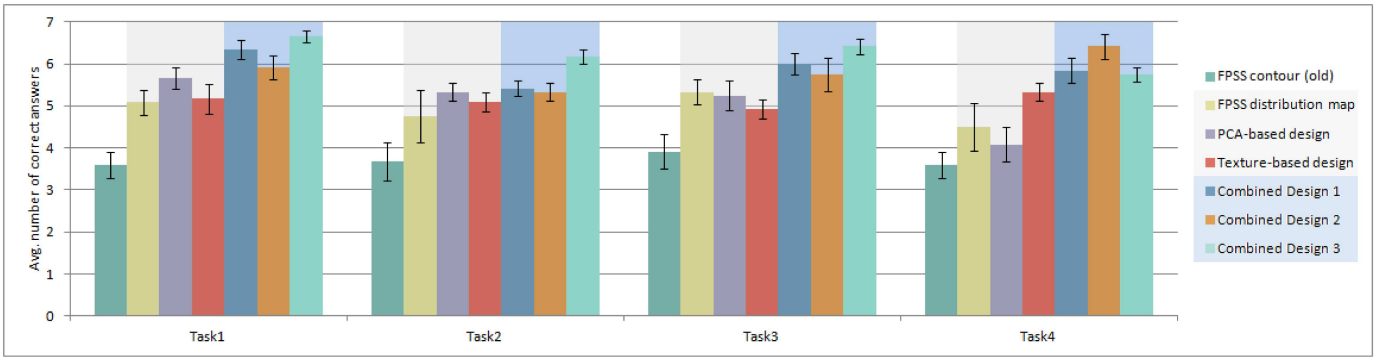

Fig. 11: The performance of the participants in the four tasks. The figure shows the average number of correct answers from the participants and error bar indicates the standard deviation of each task.

This took about 10 minutes. Detailed instructions were then given through a self-paced slide presentation. Each participant completed a total of 112 trials. This took about 30-40 minutes. When all tasks were completed, each participant completed a short debriefing questionnaire and an evaluation sheet; participants were then informed about the visual designs' related hypotheses.

6.4 Results and Discussions

Fig. 11 summarizes the average performance of the participants in relation to the four tasks mentioned in Section 6.2. (For each task, here we consider only the first four bars in the bar chart, the other three bars will be discussed in the next section.) We can observe that the performance of all new designs (i.e., FPSS distribution map, scale-space FPSS distribution map, PCA parameter boundary and Gabor-based distribution map) are on average better than the old design (i.e., FPSS contour). From Fig. 11, one may assume the relative merits of the four designs. To evaluate such assumptions, we carried out ANOVA analysis of the study results. The p-values obtained are shown in Table 1, and indicate that most comparisons between the FPSS contour and new designs are considered statistically significant. The comparisons among new designs are mostly statistically insignificant, except for Gabor vs. PCA. If we choose the p-value cutoff at 0.05, the experiment indicates the following:

- It is reasonable to conclude that all three new designs are more effective than FPSS contours (i.e., the reference design) in support Task 1, which involves deciding if an image belongs to one of the two optional classes. This is consistent with our first hypothesis.
- It is reasonable to conclude that the PCA-based and Gabor-based designs are more effective than FPSS contours in supporting Task 2, which involves deciding if an image class includes one of the two optional images. But one cannot draw conclusion regarding the FPSS distribution maps. This partially supports our first hypothesis, but indicates that questions with two image options may be harder than those with two class options. When a FPSS distribution map covers a wide range of contours, it is not so easy to exclude an image from a class.
- It is reasonable to conclude that the basic FPSS distribution map, PCA-based design and Gabor-based design are more effective than FPSS contours in supporting Task 3, which involves a decision on whether a class is a subset of another. The results however do not show that the PCA-based design is significantly better than others.
- It is reasonable to conclude that the Gabor-based design are more effective in supporting Task 4, which involves a judgment of whether images in two classes may be considered similar, while the PCA-based design appears to be less effective (contrary to our second hypothesis).

In general, this user study is helpful, showing the strength and weakness of each new design. The overall improvement of the new design upon the old design is evident.

7 Further Results

The results of the above-mentioned user study also suggest that each of the proposed designs have certain strengths and weaknesses, and they may perform better jointly. This led us to further experimentation of composite visual representations that convey different types of statistics.

7.1 Combined Visual Designs

After considering many different ways of combining the visual designs discussed in Section 5, we settled on three combined designs. The first arises from the observation that FPSS is symmetric on opposite quadrants, hence we can remove half of the redundant information and free the space for displaying other types of statistics. Gabor descriptors are shown to be effective in all four tasks. As we can observe from Fig. 9, the 1st scale (top right quadrant) and the 4th scale (top left quadrant) show most of the distinct information. This gives us the first combined design in Fig. 6(c), where the upper half of the original design for Gabor descriptors ② are combined with the lower half of the FPSS distribution map ①.

The second combined design is composed of four component regions. As shown in Fig. 6(d), the left region depicts the Gabor descriptors in the 1st and 4th scales. The right depicts 7 PCA coefficients in a manner similar to the left region to maintain certain symmetry for aesthetic reasons. The two variants of FPSS are plotted on the top and bottom regions. The bottom region is the 1st quadrant of the FPSS distribution map, except it is rotated by 135° clockwise. The top region shows a new design for FPSS that was formulated after the

	Combined Design 1				Combined Design 2				Combined Design 3			
	Task 1	Task 2	Task 3	Task 4	Task 1	Task 2	Task 3	Task 4	Task 1	Task 2	Task 3	Task 4
FPSS Distribution Map	**.009**	.12	.071	.067	.107	.239	.358	**.022**	**.001**	**.019**	**.012**	.068
PCA-based Design	.071	.777	.169	**.009**	.491	1.0	.339	**.001**	**.004**	**.025**	**.015**	**.001**
Gabor-based Design	**.015**	.266	**.002**	.275	.18	.515	**.034**	**.02**	**.004**	**.005**	<**.001**	.096

TABLE 2: Pair-wise p-values for the comparisons between the three Combined Designs and the three individual Designs discussed in Section 5 (values < 0.05 are in bold).

first user study. One drawback of the FPSS distribution map is that its stochastic and amorphous visual patterns do not convey multi-level structures effectively. We thus introduce a quantization method that first smooths the map by applying a 5×5 Gaussian filter three times and then quantizes the pixels into 4 bins. This quantized FPSS distribution map reveals some multi-level structures that are not visible in the original distribution map.

The third combined design attempts to reinstall the full set of Gabor descriptors at all four levels. As illustrated in Fig. 6(e), we plot all the Gabor lines in the outer ring ①, with a radial range [0.3, 1.2]. This allows us to use the inner circle ② of radius 0.3 for FPSS. In this case, we depict FPSS using the quantized design of distribution maps.

Figs. 12, 13 and 14 show the visualization of our 10 test classes using these three combined visual designs respectively. Fig. 15 shows the representations of 6 individual images from different image classes. The two types of statistics jointly provide visual cues to differentiate these images. For example, (i), (j) and (k) have similar Gabor patterns but FPSS sets them apart. (h) and (l) have similar FPSS patterns but Gabor descriptors sets them apart.

7.2 Further Evaluation and Discussions

With the three sets of combined visual designs as shown in Figs. 12, 13 and 14, we conducted a further user study to see if any of them can achieve better analytical performance. Following the previous user study, we compare the three Combined Designs with the original design based on FPSS contours. We adopt the same set of tasks and user interface design as in the previous user study. The same group of participants of the first experiment took part in this study. Since there was a six month gap between the two experiments and the tasks were very simple, the learning effect is insignificant. They were required to answer 84 questions, i.e., 4 tasks $\times$ 3 designs $\times$ 7 trials. The results of the study are juxtaposed with those of the first user study in Fig. 11. By comparing the last three bars with others in each task group, we can observe that the performance of all combined designs are on average better than the designs in the previous user study. We also used ANOVA analysis to evaluate assumptions about the performance of the Combined Designs that may result from Fig. 11. The last three rows of Table 1 show the p-values for comparing the Combined Designs with the FPSS contour, indicating that the relative merits of Combined Designs are conclusive. The p-values for the comparisons between the three combined designs and the three initial designs with individual statistical indicators are given in Table 2. We can observe that it is statistically significant to consider that Combined Design 3 is more effective than the three initial designs in Tasks 1, 2 and 3, and Combined Design 2 is more effective in Task 4. Among the three Combined Designs themselves, most p-values are ≥ 0.05, except Design 1 vs. Design 3 in Task 2 and Design 2 vs. Design 3 in Tasks 2 and 4. The experimental results further indicate:

- It is reasonable to conclude that all three Combined Designs are more effective than FPSS contours in supporting all four tasks.
- For Tasks 1 and 3, in particular, Combined Design 1 and 3 featuring FPSS and texture measurements outperformed other designs. The average of Combined Design 2 is higher than the three new individual designs considered in the previous study, but the comparison is not statistically significant except in Task 4. One possible reason is that extra information in this design may be slightly more confusing than Combined Designs 1 and 3.
- For Task 2, the advantages of Combined Designs 1 and 2 are not clear. Similar to the previous user study, this suggests that questions with two image options are harder than those with two class options. Nevertheless, Combined Design 3 shows noticeably better performance in supporting Task 2.
- For Task 4, which involves a judgment of whether images in two classes may be considered similar, Combined Design 2 achieved the best result. It suggests that extra statistical information may offer better support to participants in assessing the distance between classes.

In general, this further study indicates that jointly presenting different image statistics through effective visual representations can bring benefits to analytical tasks. In addition, aesthetically pleasing designs may be more effective for guiding analytical reasoning and interaction.

8 Conclusions

In this work, we have revisited the problem of visualizing image statistics with a number of new visual designs. We have followed a rigorous design process, including criteria formulation, initial designs, qualitative analysis, evaluation, further design and further evaluation. We have shown that the conventional design based on FPSS contours are not effective in supporting analytical tasks, and can sometimes be misleading, though they serve as an effective form of symbolism for image classes. It is both useful and feasible to design more effective visualization of image statistics in order to provide better support for basic analytical tasks, such as determining set memberships, subset relationships and distance between image classes. The evaluation through these basic analytical tasks suggests a more general implication in visual analysis of imagery data, for example, in terms of classification, identification of clusters and anomalies, and analysis of deviation,

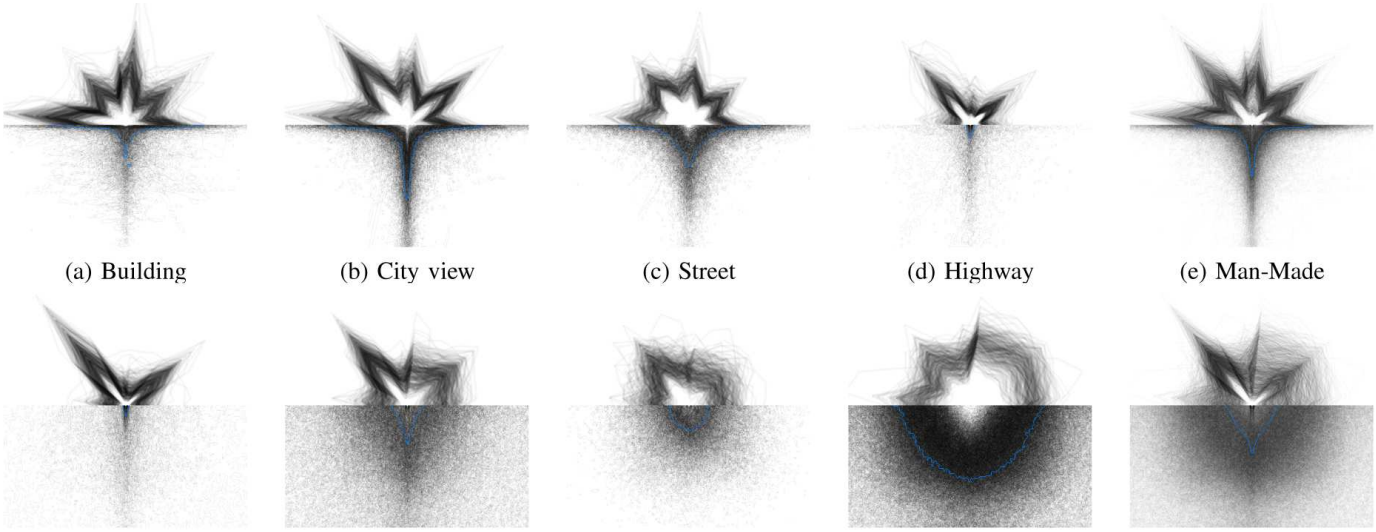

(a) Building (b) City view (c) Street (d) Highway (e) Man-Made

(f) Coast (g) Field (h) Mountain (i) Forest (j) Natural

Fig. 12: Combined Design 1 features FPSS and 8×2 Gabor descriptors.

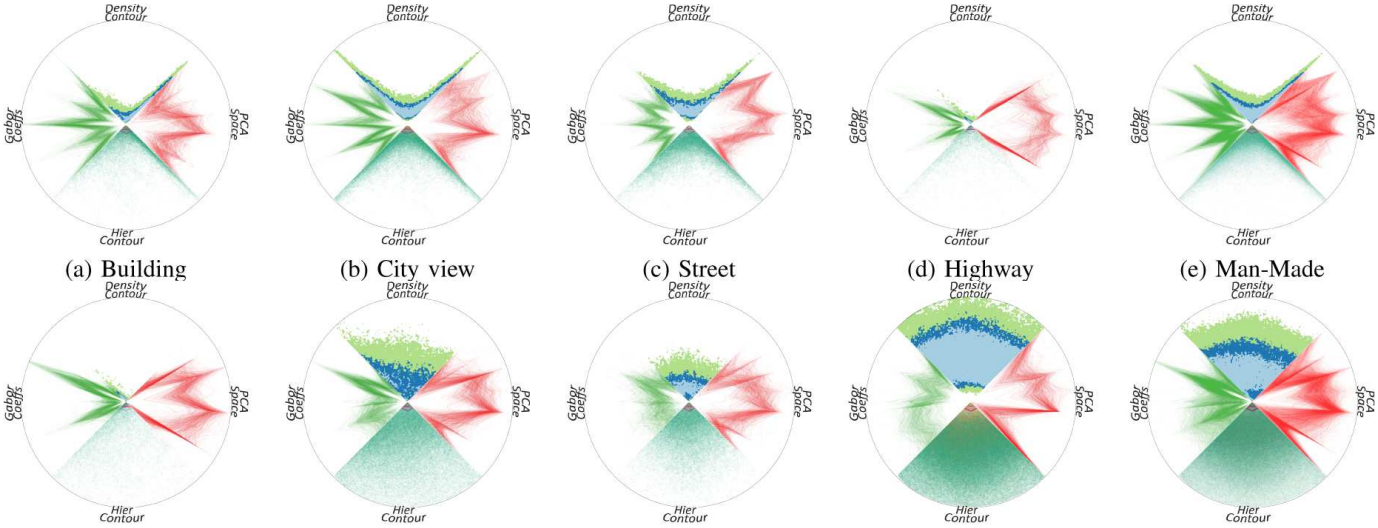

(a) Building (b) City view (c) Street (d) Highway (e) Man-Made

(f) Coast (g) Field (h) Mountain (i) Forest (j) Natural

Fig. 13: Combined Design 2 is composed of Gabor descriptors, PCA parameters, and two forms of FPSS.

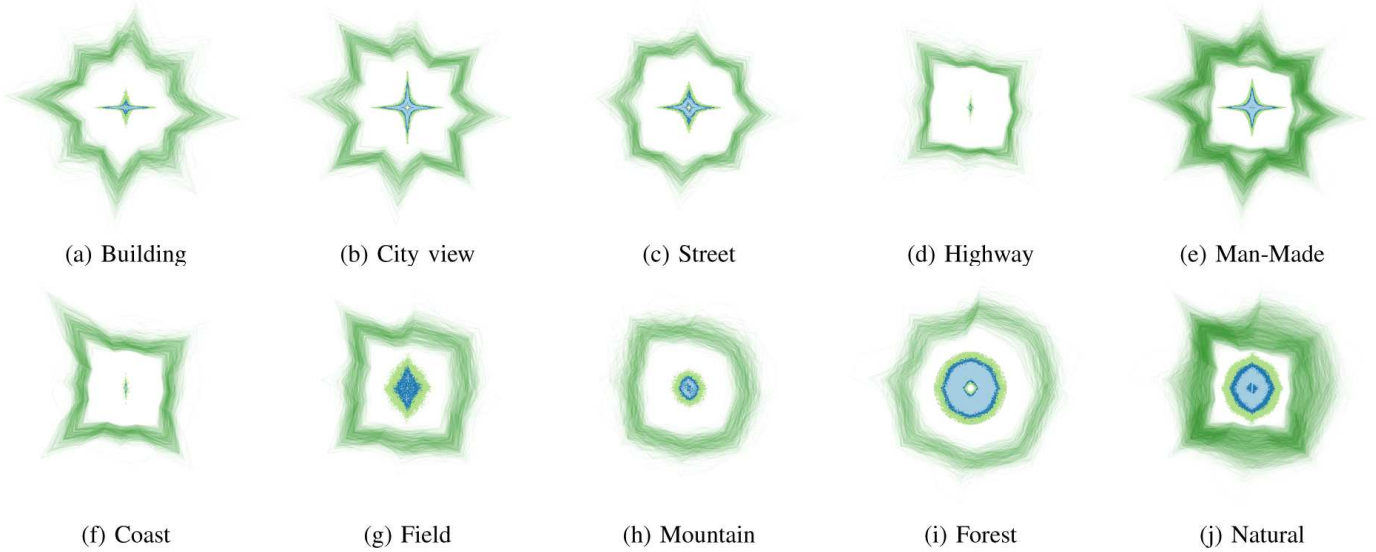

(a) Building (b) City view (c) Street (d) Highway (e) Man-Made

(f) Coast (g) Field (h) Mountain (i) Forest (j) Natural

Fig. 14: Combined Design 3 features 8×4 Gabor descriptors and quantized FPSS.

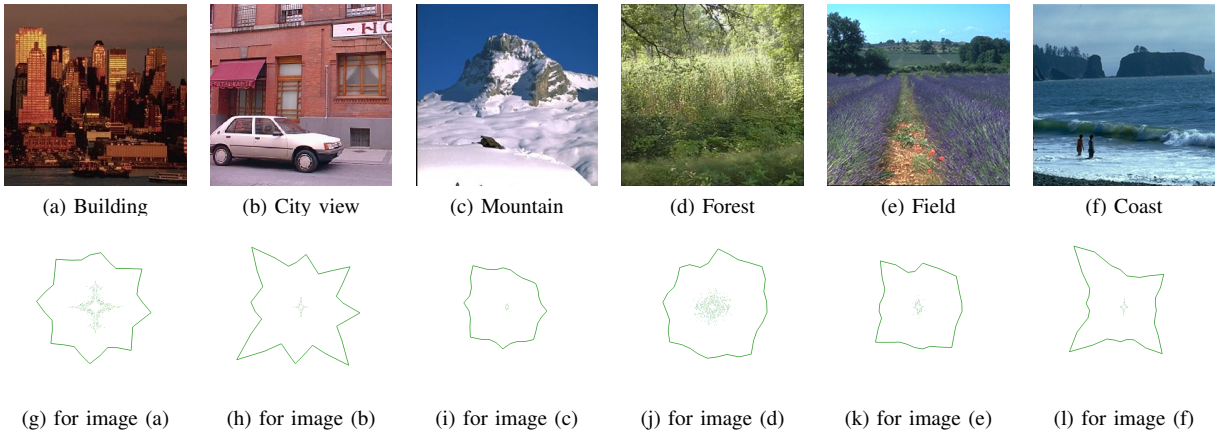

(a) Building (b) City view (c) Mountain (d) Forest (e) Field (f) Coast

(g) for image (a) (h) for image (b) (i) for image (c) (j) for image (d) (k) for image (e) (l) for image (f)

Fig. 15: Visualizing six images from different images classes using Combined Design 3.

distribution and correlation. The visual designs proposed in this paper do not require a large display space, and can easily be presented in tabular forms for various comparative tasks, or be used as visual abstraction and symbolism.

As discussed in Section 2.2, visualization of image statistics can potentially assist in many different applications of image analysis, such as categorization of painting styles, content-based image retrieval, image and video editing and so on. We plan to conduct further investigation into the use of image statistics visualization in practical applications.

REFERENCES

[1] R. Buccigrossi and E. Simoncelli. Image compression via joint statistical characterization in the wavelet domain. *IEEE Transactions on Image Processing*, 8(12):1688–1701, 1999.

[2] N. Dalal and B. Triggs. Histograms of oriented gradients for human detection. In *Proceedings of CVPR 2005*, pages 886 – 893, 2005.

[3] J. Daugman. Complete discrete 2-D Gabor transforms by neural networks for image analysis and compression. *IEEE Trans on Acoustics, Speech, and Signal Processing*, 36(7):1169–1179, 1988.

[4] O. Deussen and B. Lintermann. *Digital Design of Nature: Computer Generated Plants and Organics*. Springer-Verlag, 2005.

[5] R. O. Dror, E. H. Adelson, and A. S. Willsky. Surface reflectance estimation and natural illumination statistics. In *Proc. IEEE Workshop on Statistical and Computational Theories of Vision*, 2001.

[6] R. Fergus, B. Singh, A. Hertzmann, S. Roweis, and W. Freeman. Removing camera shake from a single photograph. *ACM Transactions on Graphics*, 25:787–794, 2006.

[7] D. Field. Relations between the statistics of natural images and the response profiles of cortical cells. *Journal of the Optical Society of America A*, 4:2379–2394, 1987.

[8] W. S. Geisler. Visual perception and the statistical properties of natural scenes. *Annual Review of Psychology*, 59:167–192, 2008.

[9] D. J. Graham and C. Redies. Statistical regularities in art: Relations with visual coding and perception. *Vision Research*, 50(16):1503–1509, 2010.

[10] I. Groen, S. Ghebreab, V. Lamme, and S. Scholte. The role of Weibull image statistics in rapid object detection in natural scenes. *Journal of Vision*, 10(7):992, 2010.

[11] S. Haroz and K.-L. Ma. Natural Visualizations. In *Eurographics /IEEE VGTC Symposium on Visualization*, pages 43–50, 2006.

[12] J. M. Hughes, Graham, D. J., and D. N. Rockmore. Quantification of artistic style through sparse coding analysis in the drawings of Pieter Bruegel the Elder. In *Proc. National Academy of Sciences USA*, volume 107, pages 1279–1283, 2010.

[13] A. Hyvärinen. Statistical models of natural images and cortical visual representation. *Topics in Cognitive Science*, 2(2):251–264, 2010.

[14] A. Hyvärinen and E. Oja. Independent component analysis: algorithms and applications. *Neural Networks*, 13(4-5):411–430, 2000.

[15] I. T. Jolliffe. *Principal Component Analysis*. Springer-Verlag, 1986.

[16] N. Katsumata and Y. Matsuyama. Database retrieval for similar images using ICA and PCA bases. *Engineering Applications of Artificial Intelligence*, 18(2005):705–717, 2005.

[17] K. Kim, M. Franz, and B. Scholkopf. Iterative kernel principal component analysis for image modeling. *IEEE Transactions on Pattern Analysis and Machine Intelligence*, 27(9):1351– 1366, 2005.

[18] A. Levin, A. Zomet, and Y. Weiss. Learning how to inpaint from global image statistics. In *Proc. IEEE International Conference on Computer Vision*, pages 305–312, 2003.

[19] R. Miller Jr. *Beyond ANOVA: Basics of Applied Statistics*. Chapman & Hall/CRC, 1997.

[20] A. Oliva and A. Torralba. Modeling the shape of the scene: a holistic representation of the spatial envelope. *International Journal of Computer Vision*, 42(3):145–175, 2001.

[21] A. Olshausen and D. Field. Sparse coding with an overcomplete basis set: A strategy employed by v1? *Vision Research*, 23(37):3311–3325, Dec. 1997.

[22] J. Portilla and E. P. Simoncelli. Image denoising via adjustment of wavelet coefficient magnitude correlation. In *Proc. 7th International Conference on Image Processing*, 2000.

[23] T. Pouli, D. Cunningham, and E. Reinhard. Image statistics and their applications in computer graphics. In *Proceedings of EUROGRAPHICS 2010*, pages 59–88, 2010.

[24] T. Pouli and E. Reinhard. Progressive color transfer for images of arbitrary dynamic range. *Computers and Graphics*, 35(1):67–80, 2011.

[25] E. Reinhard, M. Ashikhmin, B. Gooch, and P. Shirley. Color transfer between images. *IEEE Computer Graphics and Applications*, 21:34–41, 2001.

[26] E. Reinhard, P. Shirley, M. Ashikhmin, and T. Troscianko. Second order image statistics in computer graphics. In *Proceedings of the 1st Symposium on Applied perception in graphics and visualization*, APGV '04, pages 99–106, New York, NY, USA, 2004. ACM.

[27] E. Reinhard, P. Shirley, M. Ashikhmin, and T. Troscianko. Second order image statistics in computer graphics. In *Proc. 1st Symposium on Applied Perception in Graphics and Visualization*, 2004.

[28] E. Rosch, C. Mervis, W. Gray, D. Johnson, and P. Boyes-Braem. Basic objects in natural categories. *Cognitive Psychology*, 8:382–439, 1976.

[29] M. Ross and A. Oliva. Estimating perception of scene layout properties from global image features. *Journal of Vision*, 10(2):1–25, 2010.

[30] A. Torralba. Torralba outdoor scene categorization dataset. http://people.csail.mit.edu/torralba/code/spatialenvelope/.

[31] A. Torralba and A. Oliva. Depth estimation from image structure. *IEEE Transactions on Pattern Analysis and Machine Intelligence*, 24(9):1–13, Sept. 2002.

[32] A. Torralba and A. Oliva. Statistics of natural image categories. *Network: Computation in neural systems*, 14:291–412, 2003.

[33] B. Tversky and K. Hemenway. Categories of scenes. *Cognitive Psychology*, 15:121–149, 1983.

[34] A. van der Schaaf and J. van Hateren. Modelling the power spectra of natural images: statistics and information. *Vision Research*, 36(17):2759–2770, 1996.

[35] H. Wickham, D. Cook, H. Hofmann, and A. Buja. Graphical inference for infovis. *IEEE Transactions on Visualization and Computer Graphics*, 16(6):973–979, 2010.

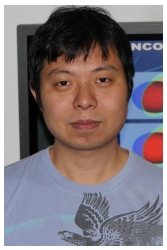

Hui Fang received his B.Sc. from Science and Technology University, Beijing, China in 2000 and Ph.D from Bradford University, UK, in 2006. He worked as a Research Associate in Manchester Metropolitan University, U.K from 2006 to 2009. He is now a research officer in Computer Science Department, Swansea University, Wales. His research interests include facial analysis, image processing and visualization and image registration and segmentation.

Gary L. Tam received his B.Eng. (first-class honors), M.Phil. and Ph.D. degrees from Hong Kong University of Science and Technology, City University of Hong Kong, and Durham University, respectively. In 2004, he worked as an instructor in the City university of Hong Kong. He is currently a research associate in the Cardiff University, United Kingdom.

Rita Borgo received her BSc and MSc (Laurea with commendation) from the University of Bologna in 2000 and PhD in Computer Science in 2004 from the University of Pisa in collaboration with the Visual Computing Lab. at the Italian National Research Council in Pisa. Since 2011 she has been a Lecturer in the Department of Computer Science, Swansea University, United Kingdom. Her research interests include volume visualization, computational geometry, hierarchical meshes and progressive algorithms, semantic web and functional languages. Lately her research has focused on video visualization and 3D image analysis and synthesis. She is a member of BCS Women in Computer Science and IEEE.

Andrew J. Aubrey received his B.Eng.(Hons) and M.Sc. in Electronic Engineering, in 2002 and 2003 respectively, and the Ph.D. in Audio-Visual Signal Processing from Cardiff University, U.K. in 2008. He is currently a research associate in the School of Computer Science, Cardiff University, U.K. His current research interests include audio visual speech processing, modelling and animation, speech separation, voice activity detection and analysis and perception of human expressions and emotions.

Philip W. Grant is a senior lecturer in the Department of Computer Science, Swansea University, UK. He received his BSc in 1968 from Manchester University, UK and obtained his DPhil in Mathematical Logic from Oxford University in 1972. His research interests include applications of genetic and logic programming, modelling of facial ageing and facial dynamics. He is a member of the IEEE Computer Society, member of the ACM and Fellow of the BCS.

Paul L. Rosin Paul L. Rosin is a Professor at the School of Computer Science & Informatics, Cardiff University. Previous posts include Brunel University, UK, Joint Research Centre, Italy and Curtin University of Technology, Australia. His research interests include the representation, segmentation, and grouping of curves, knowledge-based vision systems, early image representations, low level image processing, machine vision approaches to remote sensing, methods for evaluation of approximation algorithms, etc., medical and biological image analysis, mesh processing, and the analysis of shape in art and architecture.

Cristian Wallraven received his PhD in Physics in 2007 from University of Tbingen for work conducted at the Max Planck Institute for Biological Cybernetics on creating a perceptually motivated computer vision algorithm. In 2010, he joined Korea University as Assistant Professor and head of the Cognitive Systems Lab. His current research interests lie in the interdisciplinary intersection between computer graphics, computer vision, and the cognitive sciences. Within this, his work focuses on the cognitive and computational study of face recognition, facial expression processing, multisensory object recognition, and evaluation of computer graphics and visualization algorithms. Christian Wallraven is a member of ACM and IEEE.

Douglas Cunningham received his Ph.D in psychology from Temple University in 1997. He is currently a professor of computer science at the Brandenburg Technical University. Before joining the faculty at BTU, he was a postdoctoral researcher at the University of Tbingen, at the Max Planck Institute for Biological Cybernetics, and for Logicon Technical Services. His research interests focus on integrating psychology and computer science, and include topics such as facial expressions, image statistics, sensorimotor adaptation, and computational aesthetics.

David Marshall is a Professor in the School of Computer Science and Informatics, Cardiff University, UK. He received his BSc in 1986 from University College,Cardiff in 1986 and obtained his PhD "Three Dimensional Inspection of Manufactured Objects" from there in 1990. His research in human facial analysis, high dimensional subspace analysis, audio/video image processing, and data/sensor fusion. He has published over 130 papers and one book in these research areas. He is a member of the IEEE Computer Society and the British Machine Vision Association.

Min Chen received the Ph.D. degree from University of Wales in 1991. He is currently a professor of scientific visualization at Oxford University and a fellow of Pembroke College. Before joining Oxford, he held research and faculty positions at Swansea University His research interests include visualization, computer graphics and human-computer interaction, and has co-authored over 130 publications. His services to the research community include papers co-chair of IEEE Visualization 2007 and 2008, and co-director of Wales Research Institute of Visual Computing. He is a fellow of the BCS, Eurographics and Learned Society of Wales.